

Potential-Driven Restructuring of Cu Single Atoms to Nanoparticles for Boosting the Electrochemical Reduction of Nitrate to Ammonia

Ji Yang,[†] Haifeng Qi,[†] Anqi Li,[†] Xiaoyan Liu, Xiaofeng Yang,* Shengxin Zhang, Qiao Zhao, Qike Jiang, Yang Su, Leilei Zhang, Jian-Feng Li,* Zhong-Qun Tian, Wei Liu,* Aiqin Wang,* and Tao Zhang



Cite This: *J. Am. Chem. Soc.* 2022, 144, 12062–12071



Read Online

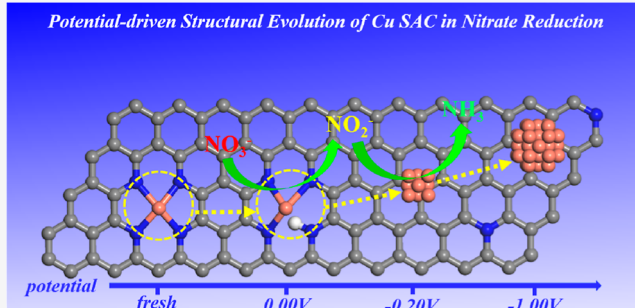
ACCESS |

Metrics & More

Article Recommendations

Supporting Information

ABSTRACT: Restructuring is ubiquitous in thermocatalysis and of pivotal importance to identify the real active site, yet it is less explored in electrocatalysis. Herein, by using *operando* X-ray absorption spectroscopy in conjunction with advanced electron microscopy, we reveal the restructuring of the as-synthesized Cu–N₄ single-atom site to the nanoparticles of ~5 nm during the electrochemical reduction of nitrate to ammonia, a green ammonia production route upon combined with the plasma-assisted oxidation of nitrogen. The reduction of Cu²⁺ to Cu⁺ and Cu⁰ and the subsequent aggregation of Cu⁰ single atoms is found to occur concurrently with the enhancement of the NH₃ production rate, both of them are driven by the applied potential switching from 0.00 to −1.00 V versus RHE. The maximum production rate of ammonia reaches 4.5 mg cm^{−2} h^{−1} (12.5 mol_{NH₃} g_{Cu}^{−1} h^{−1}) with a Faradaic efficiency of 84.7% at −1.00 V versus RHE, outperforming most of the other Cu catalysts reported previously. After electrolysis, the aggregated Cu nanoparticles are reversibly disintegrated into single atoms and then restored to the Cu–N₄ structure upon being exposed to an ambient atmosphere, which masks the potential-induced restructuring during the reaction. The synchronous changes of the Cu⁰ percentage and the ammonia Faradaic efficiency with the applied potential suggests that the Cu nanoparticles are the genuine active sites for nitrate reduction to ammonia, which is corroborated with both the post-deposited Cu NP catalyst and density functional theory calculations.



INTRODUCTION

Metal ions doped into porous nitrogen-doped carbon (M–N–C), also called M–N–C single-atom catalysts (SACs), is a class of promising electrocatalysts alternative to scarce and unaffordable noble metals in a variety of energy-related important transformations (e.g., oxygen and carbon dioxide reduction reactions).^{1,2} The high activity of M–N–C is generally attributed to the M–N_x site whose exact structure, however, remains elusive. Especially, under working conditions, the preformed M–N_x may undergo structural transformation driven by the applied potential and/or the interaction with reactants or electrolytes, which not only complicates the understanding of the structure–performance relationship but also significantly impedes the rational design of efficient catalysts. Therefore, unveiling the dynamic evolution of the M–N_x structure during electrolysis is of pivotal importance to identify the real active site. Recently, with the advance of *operando* characterization techniques, in particular *operando* X-ray absorption spectroscopy, there have been increasing examples showing that the M–N_x single-atom site structure was labile under electrochemical conditions.³ For instance, Yao and co-workers reported the transformation of the as-synthesized Co–N₄ planar structure into a high-valence

HO–Co–N₂ moiety by interacting with the electrolyte hydroxide during the alkaline hydrogen evolution reaction (HER),⁴ while Jaouen and co-workers observed the transformation of the preformed FeN₄C₁₂ into iron oxide during the oxygen reduction reaction (ORR) and this structural change was the main reason for performance degradation.⁵ Compared with Co–N_x and Fe–N_x moieties, the Cu–N_x appears more susceptible to restructuring due to the more positive standard electrode potential of Cu²⁺/Cu⁰ and Cu⁺/Cu⁰. Indeed, the reduction of Cu cations together with the morphology change was reported for various Cu-based catalysts during the electrochemical CO₂ reduction,^{6–8} and the restructuring-induced activity enhancement was also observed.^{9,10} Very recently, we have reported the dynamic evolution of Cu–N–C SAC during ORR from the original Cu²⁺–N₄ to Cu⁺–N₃ and further to the HO–Cu⁺–N₂ structure with the applied

Received: March 1, 2022

Published: June 29, 2022



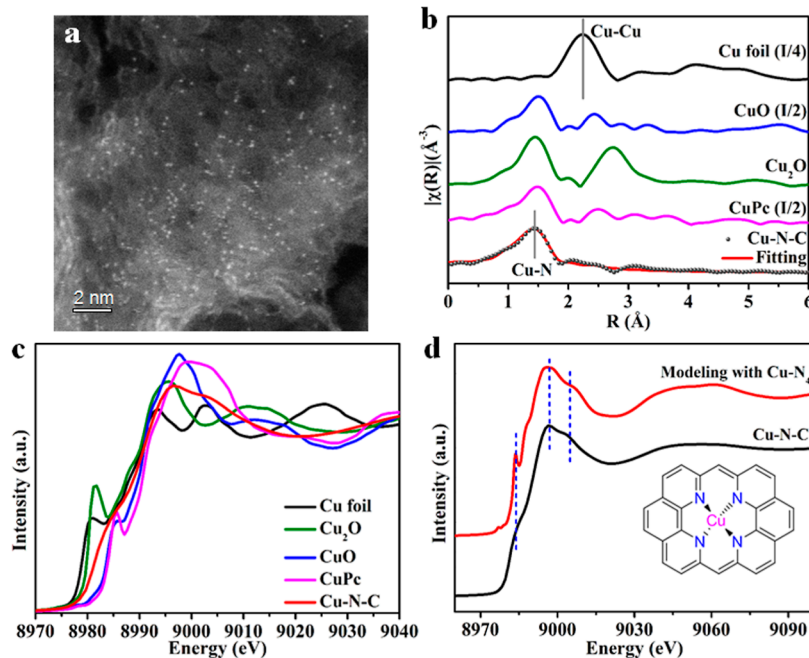


Figure 1. Structural characterizations of Cu–N–C SAC. (a) Atomic-resolution HAADF-STEM image. (b) FT-EXAFS spectra of the Cu–N–C catalyst and reference samples including Cu foil, Cu₂O, CuO, and CuPc. (c) Cu K-edge XANES spectra of Cu–N–C and reference samples including Cu foil, Cu₂O, CuO, and CuPc. (d) Comparison between the experimental spectrum of Cu–N–C (black line) and the theoretical spectrum of the Cu–N₄ model (red line, inset, Cu–N₄ structure).

potential switching from 1.1 to 0.1 V, and identified the latter two structures were more favorable to ORR.¹¹

Electrochemical fixation of nitrogen (N₂) powered by renewable energy has emerged as a promising approach toward green ammonia synthesis alternative to conventional high energy-consuming^{12,13} and CO₂-emission¹⁴ Haber–Bosch process. Nevertheless, the high dissociation energy of N≡N (941 kJ mol⁻¹) and the limited solubility of nitrogen in the aqueous solution lead to unacceptably low ammonia selectivity and productivity in electrochemical nitrogen fixation.^{15,16} To overcome the intrinsic barrier of the direct electrolysis of N₂, we recently proposed a “plasma-electrocatalysis” strategy¹⁷ by mimicking one of the natural nitrogen cycles, in which the nitrogen is first oxidized by non-thermal plasma to reactive nitrogen species (RNS) which is usually presented as water-soluble nitrate/nitrite species in aqueous electrolytes,¹⁸ and then, the produced RNS is converted into ammonia with a high selectivity and efficiency via electrochemical reduction. Therefore, it is keenly desired to develop highly selective and durable electrocatalysts for RNS reduction to ammonia. However, one challenge associated with this electrochemical transformation involving the 8e⁻/9H⁺ transfer process is the selectivity control because the reduction reaction may stop at any intermediate step depending on the catalyst structure as well as the applied potential.^{19–21} M–N–C SACs with a well-defined M–N_x structure have shown great potentials in steering the nitrate reduction toward ammonia based on recent reports.^{22–26} However, it remains an open question whether the pre-formed M–N_x structure is stable at highly reducing conditions applied, and if not, what is the genuine active site structure for this demanding electrochemical process?

Herein, with Cu–N–C SAC as a model catalyst and *operando* X-ray absorption spectroscopy as the technique, we present a detailed study on the evolution of active sites during

the electrochemical reduction of nitrate. With the applied potential moving from 0.00 to −1.00 V versus RHE, the as-synthesized Cu–N₄ structure underwent successive transformations from Cu–N₃ to near-free Cu⁰ single atoms and eventually to aggregated Cu⁰ nanoparticles. Concomitantly, the ammonia production rate was steadily enhanced until the maximum of 4.5 mg cm⁻² h⁻¹ (12.5 mol_{NH₃} g_{Cu}⁻¹ h⁻¹) with a Faradaic efficiency (FE) of 84.7% was reached at −1.00 V versus RHE. The synchronous change of the Cu⁰ percentage with the ammonia production rate suggests the potential-induced evolution of Cu⁰ nanoparticles are the genuine active sites, which is further supported by both the post-deposited Cu NPs catalyst and density functional theory (DFT) calculations. Moreover, the as-evolved Cu⁰ nanoparticles can be disintegrated into single atoms and again restored to the Cu–N₄ structure upon being exposed to an ambient atmosphere after the electrolysis, which highlights the great importance of the *operando* characterizations.

RESULTS AND DISCUSSION

Synthesis of Cu–N–C SAC and Electrochemical Performance. The Cu–N–C SAC was synthesized with a modified procedure according to our previously reported two-step approach (Figure S1).¹¹ The as-synthesized Cu–N–C is featured with a large surface area (1065 m² g⁻¹), a high N content (10.23 at. % N), and a mesoporous structure (Table S1 and Figures S2 and S3). The Cu concentration in the Cu–N–C is determined to be 1.0 wt % by inductively coupled plasma optical emission spectroscopy. The single-atom dispersion of Cu is visualized by aberration-corrected high-angle annular dark-field scanning transmission electron microscopy (HAADF-STEM) imaging (Figure 1a and more images see Figure S4), which is further corroborated with the absence of the Cu–Cu scattering path in the extended X-ray absorption fine structure (EXAFS) spectrum (Figure 1b). The

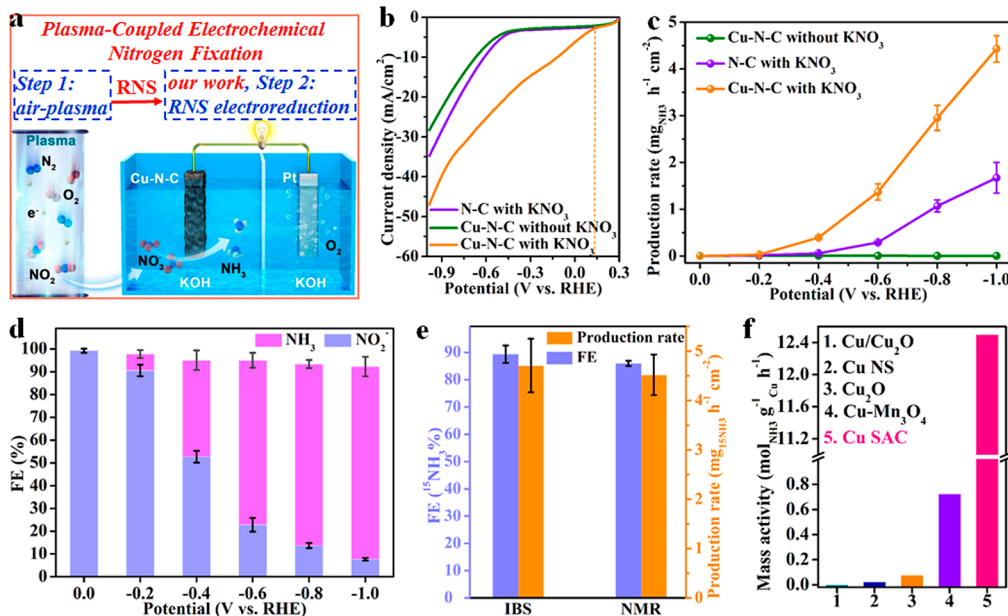


Figure 2. Electrocatalytic performance of Cu–N–C SAC. (a) Schematic illustration of green synthesis of ammonia by coupling plasma-assisted N₂ activation and electrochemical nitrate reduction. (b,c) LSV polarization curves and ammonia production rate over N–C and Cu–N–C catalysts in 0.1 M KOH electrolyte with or without nitrate. (d) FE of ammonia and nitrite products at different applied potentials. (e) FE and production rate of ¹⁵NH₃ at -1.00 V vs RHE determined by IBS and NMR, respectively. (f) Comparisons of metal mass activity of Cu–N–C SAC with the other Cu ensemble catalysts reported recently.

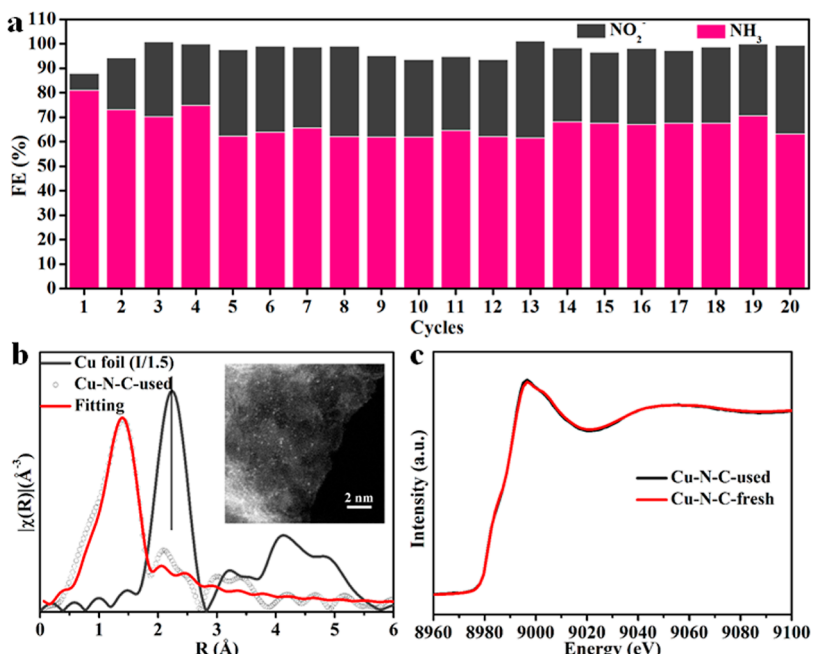


Figure 3. Durability measurements. (a) Nitrate reduction for 20 electrolysis cycles at -1.00 V vs RHE. (b) Corresponding FT-EXAFS spectra and HAADF-STEM image (inset) after durability measurements. (c) Cu K-edge XANES comparison between fresh and used Cu–N–C catalyst after durability measurements.

EXAFS fitting results show the Cu–N–C SAC has a Cu–N₄ structure with a Cu–N bond length of 1.92 Å (Figure S5 and Table S2), which is further confirmed by the X-ray absorption near-edge spectroscopy (XANES) modeling based on a finite difference method near-edge structure calculation^{27–29} (Figure 1c,d), similar to our previous report.¹¹ Then, the as-synthesized Cu–N–C SAC was evaluated for electrochemical nitrate reduction, which is considered as an alternative method for the green synthesis of ammonia by coupling with the

“plasma-assisted N₂ activation” proposed recently by our work (Figure 2a).¹⁷ The electrochemical activity of the Cu–N–C SAC toward nitrate reduction was performed in an alkaline solution of 0.1 M KOH at room temperature and atmospheric pressure. The product ammonia was quantified by indophenol blue spectrophotometric (IBS) method and further confirmed by NMR using ¹⁵N isotope labeled nitrate as the reactant, while the intermediate nitrite was quantified by the Griess test (for experimental details, see the Supporting Information, and

for the calibration curves, see Figures S6–S8). The linear sweep voltammetry (LSV) polarization curves of the N–C support and Cu–N–C SAC, with and without the presence of 0.1 M KNO₃, are shown in Figure 2b. As one can see, by adding nitrate into the electrolyte, the Cu–N–C SAC presents a much higher current density than the parent N–C support, with a greatly enhanced onset potential (0.136 V vs RHE) as compared with that in absence of nitrate (−0.5 V vs RHE). Moreover, the maximum production rate of ammonia over the Cu–N–C SAC is almost threefold larger than that on the parent N–C support (Figure 2c), indicating that Cu plays a catalytic role in the electro-reduction of nitrate to ammonia.

The potential-dependent FEs of ammonia and nitrite products are displayed in Figure 2d. It can be seen that the electrochemical reduction of nitrate over the Cu–N–C experiences a two-electron transfer process ($\text{NO}_3^- + 2\text{e}^- + \text{H}_2\text{O} \rightarrow \text{NO}_2^- + 2\text{OH}^-$) at the initial potential of 0.00 V versus RHE, as indicated by a nearly 100% FE of nitrite byproduct with an ultrahigh production rate (3.6 mg cm^{−2} h^{−1}, Figure S9) at this potential. However, the further decrease of cathodic potential leads to a continuous increase of the ammonia FE accompanied with the decrease of the nitrite FE. In particular, when the cathodic potential is decreased from −0.20 to −0.40 V versus RHE, the FE to ammonia production is enhanced from 7.2 to 42.4%, almost by sixfold. At the potential of −1.00 V versus RHE, the ammonia production predominates with a FE of 84.7% and a rate of 4.5 mg cm^{−2} h^{−1} (Figure 2c,d). Moreover, both the FE and the ammonia production rate at −1.00 V versus RHE were confirmed by NMR using the ¹⁵N isotope labeled nitrate as the reactant, and they were very close to those determined by IBS (Figure 2e), thus excluding the possibility of the N constituent in the catalyst participating into the reaction. In addition to ammonia, a small amount of H₂ was also formed at applied negative potentials with a FE less than 10%, indicating that HER has been greatly suppressed. The Cu–N–C SAC exhibited a quite high metal mass yield of 12.5 mol_{NH₃} g_{Cu}^{−1} h^{−1} at −1.00 V versus RHE (Figure 2f), this rate, to the best of our knowledge, is at least 1 order of magnitude higher than most of those Cu catalysts such as Cu/Cu₂O nanowire arrays (<0.001 mol_{NH₃} g_{Cu}^{−1} h^{−1}),³⁰ Cu nanosheets (0.023 mol_{NH₃} g_{Cu}^{−1} h^{−1}),³¹ Cu₂O (0.0786 mol_{NH₃} g_{Cu}^{−1} h^{−1}),³² and Cu–Mn₃O₄ (0.726 mol_{NH₃} g_{Cu}^{−1} h^{−1})³³ reported thus far (Table S3).

The durability of the Cu–N–C catalyst was examined for the continuous 20 cycles at an operation potential of −1.00 V versus RHE in an alkaline electrolyte. As shown in Figure 3a, the FE of ammonia had a slight decrease in the initial three cycles then leveled off at 72% in the subsequent 17 cycles. Meanwhile, the current density increased greatly in the initial three cycles, together with the remarkable enhancement in the nitrite yield (Figure S10). This phenomenon suggests that the Cu–N–C SAC might be activated during the initial stage, which is probably caused by the restructuring of the single-atom precursor. To our surprise, however, the Cu–N₄ structure with single-atom dispersion appears to keep unchanged as evidenced by both the HAADF-STEM and XAS characterizations on the used catalyst (Figures 3b,c and S11 and Table S2).

Structural Dynamics and Active Site Evolution. The switch of the reaction path from nitrite to ammonia with the decrease in the cathodic potential as well as the remarkable activity increase in the initial several cycles may imply the

structure change driven by the applied potential, taking into account that the Cu–N₄ transforms into Cu–N₃ and Cu–N₂ during the ORR as we recently reported.¹¹ In order to monitor the structural evolution of the Cu–N–C SAC with the descending of the cathodic potential, we performed *operando* XAS experiments at the Cu K-edge (measurement details see the Supporting Information). The XANES spectra of the Cu–N–C at different applied potentials show a prominent decline in the edge energy as compared to the fresh catalyst, and continue decreasing with the applied potential moving negative (Figures 4a and S12), indicating the occurrence of the

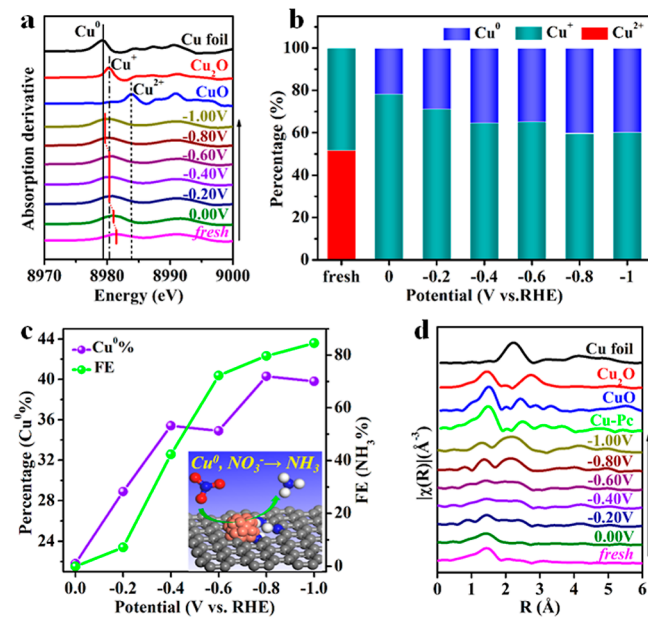


Figure 4. *Operando* XAS measurements. (a) First-order derivatives of the XANES spectra recorded at different cathodic potentials in nitrate electrolysis. (b) LCF result of the Cu K-edge XANES spectra at different potentials. (c) Potential-dependent FE and Cu⁰ percentage (inset is the evolved Cu⁰ active site toward ammonia synthesis). (d) Corresponding Cu K edge FT-EXAFS spectra at different potentials from fresh, 0.00 to −1.00 V vs RHE.

reduction of Cu²⁺/Cu⁺. It is noted that the fresh catalyst already includes a great portion of Cu⁺ estimated to be 48.3% according to the linear combination fitting (LCF) on the XANES spectrum of the fresh sample (Figure S13 and Table S4). Such abundance of Cu⁺ is supposed to form during the second pyrolysis under an inert atmosphere (see Supporting Information, catalyst preparation), which is supported by the XAS characterization result before and after the pyrolysis (Figure S14).³⁴ More interestingly, when the XANES spectra at each applied potential are fitted by the similar method (Figure S15), it is found that they are all composed of Cu⁰ and Cu⁺ (Figure 4b). Obviously, the applied potential has a profound impact on the ratio of Cu⁺/Cu⁰; more negative potential results in more Cu⁰. Nevertheless, even at the potential of −1.00 V versus RHE, there are approximately 60% of the total Cu remaining at Cu⁺ (Table S4). Among them, 48.3% Cu⁺ already present in the fresh catalyst should be encapsulated or imbedded in the N-doped carbon support during the catalyst preparation and thus be protected from the further reduction by applied potential. The contribution of this portion of inaccessible Cu⁺ to the nitrate reduction is minor according to the control test with the acid-leached sample

(Figure S16). The other ~10% Cu⁺ is probably formed at the solid–liquid interface as the result of the strong alkaline environment which is conductive to create a dynamic equilibrium between Cu⁰ and Cu⁺.³⁵ Therefore, except for the imbedded Cu⁺ species, the remaining *ca.* 50% Cu species participates in the reaction. When correlating with the catalytic selectivity, the same trend of the Cu⁰ percentage and the FE_{NH₃}, with the applied potential leads to the conclusion that the Cu⁰ plays a major role in the electroreduction of nitrate to ammonia (Figure 4c).

The Fourier-transforms of the EXAFS (FT-EXAFS) spectra are displayed in Figure 4d, and the best-fit EXAFS parameters are given in Table S5. As compared to the fresh sample that is featured with the Cu–N₄ structure, the coordination number (CN) of Cu–N/O in the first shell had a clear decrease from 3.7 to 2.8 upon the sample was subject to electrocatalysis at the applied potential of 0.00 V versus RHE, which is in agreement with our previous report that the Cu–N bond is partially broken.¹¹ Although the XANES fitting indicates that Cu⁰ accounts for 21.8% at this potential, neither the Cu–Cu peak near 2.4 Å is visible nor the Cu–Cu contribution is present in the best-fit result, which strongly indicates that the aggregation of Cu⁰ occurs, if any, to a negligible degree. This result seems to imply the formation of near-free Cu single atoms, as earlier reported near-free Pt single atoms³⁶ formed during HER and near-free Ni single atoms³⁷ during ORR. Correlating with the production rate of ammonia at this potential, we tend to believe that the single atoms of Cu, either Cu⁺ or Cu⁰, is inactive to the ammonia production, and this will be further consolidated with a controlled experiment below. On the other hand, with the applied potential moving more negative, the Cu–Cu peak develops gradually until the applied potential arrived at –0.60 V versus RHE and dramatically increases in the intensity at the potential of –0.80 to –1.00 V versus RHE. Concurrently, the peak of Cu–N attenuates at first and then abruptly gets intensified at –0.80 to –1.00 V versus RHE. The best-fit results in Table S5 reveal that the Cu–N CN decreases from 2.8 to 1.8, while the Cu–Cu CN rises from 0 to 3.7. If considering approximately 40% Cu⁰ at the potential of –0.80 and –1.00 V versus RHE, the real CN of Cu–Cu would reach 7.0 and 9.3, respectively. Evidently, significant aggregation of Cu took place when more negative potential was applied.³⁸ The structural transformation from single atoms to nanoparticles is also indicated by the significant decrease of the electrochemically active surface area from 443.2 cm² of the fresh catalyst to 146.2 cm² of the post-electrolysis catalyst (Figure S17). Coincidentally, both the activity and selectivity to ammonia production arrive at the highest values at the potential of –1.00 V versus RHE. This may lead to a conclusion that the large nanoparticles of Cu are more favorable than the single atoms for this target reaction (inset in Figure 4c). This will be addressed further below. The above *operando* XAS experiments unambiguously demonstrate that the single atoms of Cu are unstable under negative potentials and subject to reduction to Cu⁰ and then aggregation to large particles driven by the applied potentials. A control *operando* XAS experiment without nitrate shows almost identical XANES spectra at –1.00 V versus RHE, but the Cu–Cu peak in the EXAFS spectra in R-space becomes less strong (Figure S18), indicating the restructuring of Cu single atoms to NPs is driven by the applied potential, and the

electrochemical reduction of nitrate promotes the aggregation to some extent.

Nevertheless, the used catalyst restores the Cu–N₄ structure as indicated by the ex situ EXAFS experiment, as exhibited in Figure 3b,c. To figure out if the above potential-driven structure change is reversible, we switched the applied potentials from –1.00 back to 0.00 V versus RHE. Unexpectedly, however, both the EXAFS and XANES spectra remain the same (Figure 5a) and the Cu–Cu metallic bonding

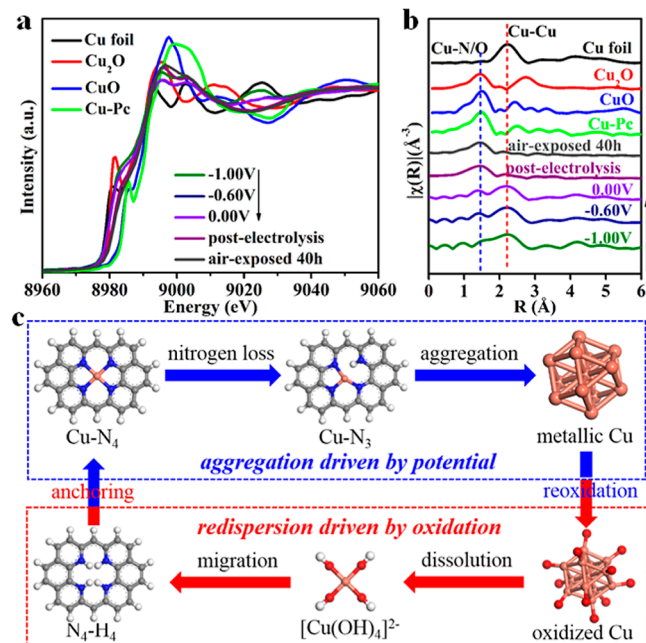


Figure 5. (a) Cu K-edge XANES spectra at different potentials from –1.00 to 0.00 V vs RHE. (b) Cu K edge FT-EXAFS spectra by switching potentials from –1.00 to 0.00 V vs RHE. (c) Proposed mechanisms of aggregation driven by the applied potential and re-dispersion in the oxidation environment.

is evident in the FT-EXAFS spectra (Figure 5b). This result indicates that the big Cu nanoparticles, upon being formed, cannot be dis-integrated by merely applying the potential until 0.00 V versus RHE. Therefore, there must be other factors than the applied potential giving rise to the disintegration of Cu particles. In order to unveil the process, we directly removed the applied potential and then recorded the EXAFS spectra at different durations. It is found that the EXAFS spectrum of the catalyst after the electrolysis (labeled as “post-electrolysis”) exhibits a partially restored peak at 1.45 Å characterizing the Cu–N scattering path, which is consistent with the incomplete reversibility observed in the XANES spectrum (Figure S19). Meanwhile, the LCF of the XANES spectra reveals 56.1% Cu⁺, 9.7% Cu⁰, and mixed with 34.3% Cu²⁺ in the post-electrolysis catalyst (Table S4), indicating the possible formation of oxidized Cu with a smaller particle size.³⁹ This result seems to suggest that oxygen⁴⁰ and/or water⁴¹ in air may play a role in the re-dispersion of large Cu NPs. To prove this hypothesis, the post-electrolysis sample was further allowed for exposure in air for *ca.* 40 h. As expected, both the XANES and FT-EXAFS spectra at this stage replicate completely those of the fresh sample (Figure S20). Therefore, the disintegration of the Cu NPs to single atoms can be accomplished in the oxidative environments, possibly via

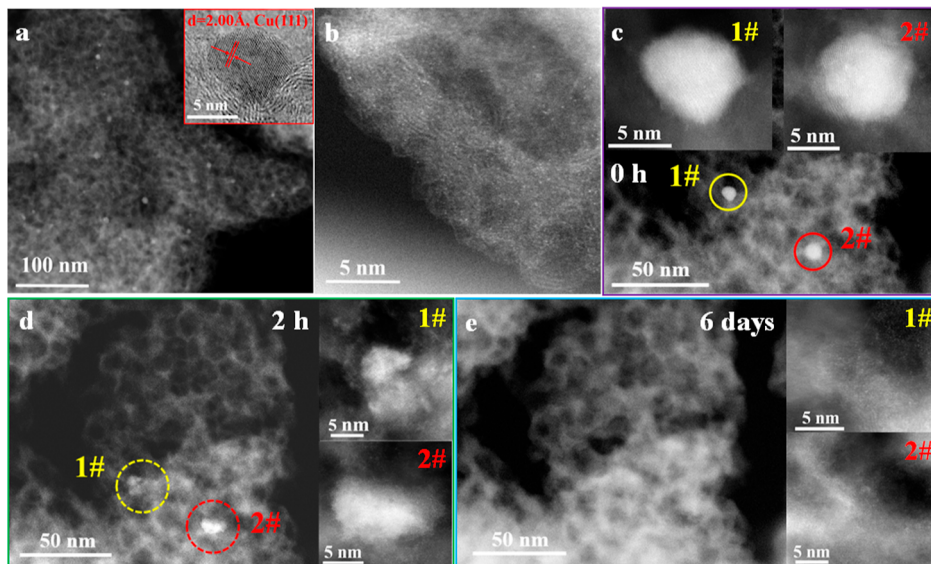


Figure 6. Identical-location electron microscopic characterizations. (a,b) HAADF-STEM images of the argon-protected Cu–N–C sample after nitrate electrolysis at -1.00 V vs RHE for 1 h showing the co-existence of NPs and single atoms. The inset is an enlarged image showing the lattice fringe of Cu(111). (c–e) The HAADF-STEM images of individual particles labeled as Cu1# and 2# immediately after the electrolysis as well as after exposure to air for 2 h and 6 days, respectively.

$[\text{Cu}(\text{OH})_4]^{2-}$ intermediate⁴² which is subsequently trapped by pyridinic nitrogen on the carbon support (Figure 5c).¹¹ The complete recovery of the initial Cu–N₄ structure is also approved by the nitrate electrochemical reduction test which shows almost identical current density, ammonia production rate, and FE obtained on the above “post-electrolysis and air-exposed 120 days” sample to those on the fresh Cu–N–C catalyst (Figure S21). It should be noted that the N-doped carbon backbone remained well after electrolysis, which is supported by both the nitrogen adsorption–desorption isotherms and N 1s XPS spectra (Figures S22 and S23 and Table S6). Such a good stability of the N–C structure offers a prerequisite for restoring the Cu–N₄ structure. The shuttle between isolated Cu²⁺ single atoms and aggregated Cu⁰ NPs which is forward driven by the applied potential and reversed back in oxidation environment underlines the extreme importance of the *operando* characterization of the catalyst; otherwise, one would believe that the Cu–N_x single-atom structures are the active sites as proposed in the literature.^{22,23,25,43}

The above reversible restructuring is further confirmed with identical-location TEM examinations. To avoid the interference of fragmentation of the Cu particles upon air exposure, the electrocatalytic test and TEM sample preparation were all performed in the glovebox under the protection of an argon atmosphere. Representative images are shown in Figures 6a and S24. The Cu NPs with sizes of 5–10 nm are evidently observed in the HAADF-STEM images of the post-electrolysis sample, which is well consistent with the EXAFS results that significant aggregation of Cu⁰ took place driven by the applied potential of -1.00 V versus RHE. Meanwhile, a large portion of Cu residing in uniform dispersion of single atoms is also visible in aberration-corrected HAADF-STEM imaging as shown in Figures 6b and S25, implying that these Cu single atoms should be imbedded into and/or constrained onto the carbon support and therefore cannot be reduced into particles by the applied potential, which coincides with the XANES and EXAFS analysis showing that around 60% Cu remained as

isolated Cu⁺ after the electrocatalytic test at -1.00 V versus RHE. To explore the evolutionary behaviors of Cu NPs in the ambient atmosphere, we allowed the reaction-formed sample to air exposures for 2 h and 6 days, respectively. A prominent trend of disintegration is clearly demonstrated for fresh particles 1# and 2# after exposure to air for 2 h (Figure 6c,d). The disintegration rate of the smaller particle 1# is remarkably higher than the larger 2#. After air exposure of 6 days (Figure 6e), none of the particles could be found in the same area, indicative of the complete fragmentation into single atoms. It is worth noting that the air exposure triggers remarkably high efficiency of Cu dispersion even under this circumstance of solid reaction, whereas a more instant restructuring would be expected given in the practical liquid environment of electroreduction.

Electrolysis Mechanism of Nitrate Reduction. Based on the experimental results, we can draw a reliable conclusion that the as-synthesized Cu–N₄ SAC cannot survive under the applied negative potentials, and the evolution of Cu nanoparticles concurrently takes place with the production of ammonia. Nevertheless, as both the reduction of nitrate to NH₃ and the reduction of Cu²⁺ to Cu⁰ are driven by the applied negative potential, it is mandatory to disentangle the structural evolution from the effect of applied potential on the reaction. To this end, we first designed several control experiments to see if there is size effect in the electroreduction of nitrate. The results shown in Figure S26a demonstrate that the large Cu particles (CN_{Cu–Cu} is calibrated as 9.3) which are formed by pretreating at -1.00 V versus RHE are inactive at all at 0.00 V versus RHE, indicating that the reductive reaction of nitrate to ammonia can only proceed at negative potentials, irrespective of Cu single atoms or NPs. Therefore, we chose a moderate reductive potential of -0.60 V versus RHE to compare the catalyst with different sizes. The large-size catalyst (CN_{Cu–Cu} 9.3) gave rise to 75% FE of NH₃ at the applied potential of -0.60 V versus RHE, which is corresponding to the ammonia yield of $18.5\text{ mol g}_{\text{Cu}^0}^{-1}\text{ h}^{-1}$. In contrast, the small clusters (Cu–Cu CN is calibrated as 5.7) which is

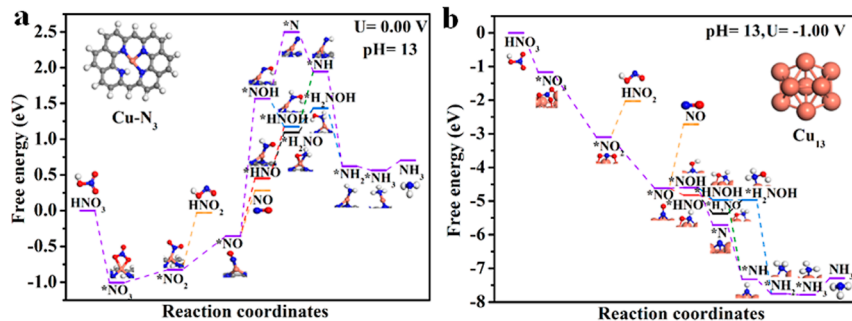


Figure 7. DFT calculations. The free energy diagrams for electrochemical nitrate reduction to ammonia and nitrite on Cu–N₃ (a) and Cu₁₃ (b) sites, respectively.

formed by pretreating at −0.60 V versus RHE, leads to a slightly higher ammonia yield of 19.5 mol g_{Cu0}⁻¹ h⁻¹ at the same potential (Figure S26b,c). Obviously, the size effect of metallic Cu NPs in a certain range (<10 nm) is not significant for this reaction. To further confirm this point, we also prepared a Cu NPs/N–C control sample by reducing Cu²⁺ to Cu NPs with NaBH₄ and then deposited onto the preformed N–C support. In spite of larger sizes of Cu particles (Figure S27) in this sample, it delivered almost the same NH₃ production rate as the Cu–N–C catalyst (Figure S28). Nevertheless, the FE of ammonia is lower due to the higher selectivity to nitrite on the Cu NPs/N–C catalyst, which may reflect some advantage of the in situ formed NPs during the electrolysis.

Subsequently, to get an atomic insight into the reaction mechanism of nitrate reduction, we have performed DFT calculations on the thermodynamic elementary steps of the electron/proton coupling from nitrate to ammonia over Cu–N₃ SAC and Cu₁₃ metallic cluster, at the applied potentials of 0.00 and −1.00 V versus RHE, respectively. Various possible intermediates inferred from nitrate reduction have been considered on Cu active centers in electrolysis. As such, the routes of nitrate electroreduction to nitrite derived from NO₂* intermediate, as well as to gaseous NO from NO* species are surveyed to understand the selectivity trends at different applied potentials. The nitrite as the reaction intermediate is supported by the experimental concentration–time curve in which the nitrite concentration shows a volcano-shape, whereas the ammonia increases monotonously with the reaction time (Figure S29). Moreover, the electrochemical reduction of nitrite produces a much higher ammonia production rate and FE than the nitrate reduction (Figure S30), which also suggests nitrite as the intermediate. Meanwhile, different reduction pathways for *NO to NH₂* are explored in terms of the possible proton hydrogenation through O or N endpoints of NO* intermediate. It can be seen that (Figure 7a), the reduction of nitrate to NO₂* is greatly favorable over the Cu–N₃ catalyst, and the generation of nitrite is nearly in a thermodynamic neutrality (−0.03 eV) at the applied potential of 0.00 V versus RHE. However, the further reduction of NO₂* intermediate to NO as the gaseous product is less favorable, with an endothermic energy of 0.28 eV. Moreover, the electroreduction of NO* to ammonia suffers a great thermodynamic difficulty. Even through the most feasible proton transfer route of *NO to HNO*, H₂NO*, and *H₂NOH as the highest thermodynamic intermediate obstacle, it should go over a thermodynamic barrier as high as 1.43 eV. As a result, it leads to the main selectivity toward

nitrite over the Cu–N₃ SAC catalyst at the applied potential of 0.00 V versus RHE, which is in line with the experiment results.

By contrast, the electroreduction of nitrate over the Cu₁₃ cluster at −1.00 V versus RHE presents a distinctive energy landscape (Figure 7b). The elementary steps for nitrate to ammonia experience a successive decline in thermodynamics; only the desorption of ammonia has a slight endothermic energy of 0.48 eV. In comparison, the reduction to nitrite and NO byproducts encounter a much higher endothermic energy, with values of 1.07 and 1.90 eV, respectively. It thus suggests the preferable generation of ammonia instead of nitrite during the electroreduction of nitrate over the metallic Cu nanocatalyst at −1.00 V versus RHE, in accordance with our experimental findings. Similar to that over the Cu SAC, the proton transfer of *NO occurs through the HNO* and HNOH* intermediates, while the further reduction can be realized in two pathways, that is, through the H₂NOH* or NH* intermediates to H₂N*, and finally to ammonia. Moreover, the applied potential plays a critical role on the electron/proton coupling in the N–O bond cleavage and the hydrogenation of NH_x* to NH₃*, which requires a more negative applied potential for a high electrolysis activity in nitrate to ammonia.

CONCLUSIONS

While the M–N–C SAC has been extensively investigated in electrochemical transformations, the structure evolution during the reaction is less explored. In this work, by using *operando* XAS we provide strong evidence that the as-synthesized Cu–N₄ structure underwent successive transformations to Cu–N₃, near-free Cu⁰ single atoms, and eventually to aggregated Cu⁰ nanoparticles during the electrochemical reduction of nitrate when the applied potential was changed from 0.00 to −1.00 V versus RHE. Concurrently with the evolution of Cu⁰ nanoparticles, the ammonia production rate was enhanced greatly. This synchronous change suggests that the reaction-induced Cu⁰ nanoparticles, instead of the as-synthesized Cu–N₄ structure, are the real active sites. Moreover, after electrolysis, the aggregated Cu⁰ nanoparticles can be disintegrated into single atoms and then restored to the Cu–N₄ structure upon being exposed to an ambient atmosphere, as demonstrated by both XAS and HAADF-STEM imaging. The shuttle between isolated Cu–N₄ single-atom sites and aggregated Cu⁰ nanoparticles, which is forward driven by the applied potential and back driven by the oxidation environment, underlines the paramount importance of the *operando* characterization of the catalyst. Owing to the potential-driven

evolution of the active Cu⁰ nanoparticles, the catalyst gave rise to the maximum ammonia production rate of 4.5 mg cm⁻² h⁻¹ (12.5 mol_{NH₃} g_{Cu}⁻¹ h⁻¹) with a FE of 84.7% at -1.00 V versus RHE, which promises for the green synthesis of ammonia when combined with the plasma-assisted oxidation of nitrogen.

ASSOCIATED CONTENT

Supporting Information

The Supporting Information is available free of charge at <https://pubs.acs.org/doi/10.1021/jacs.2c02262>.

Detailed catalysts synthesis; characterization methods; schematic illustration of the Cu–N–C synthetic procedure; N₂ adsorption–desorption isotherms; pore size distribution of the Cu–N–C catalyst; XPS characterizations; HAADF-STEM images; FT-EXAFS fitting curve; absorption curves; concentration–absorbance calibration curves; ¹H NMR spectra; nitrite production rate; durability measurements; Cu K-edge XANES spectra; LCF results; LSV polarization curves; electrochemical capacitance measurements; XAS comparisons; high-resolution N1s spectra; SEM images; comparison of the nitrate reduction to nitrite reduction; atomic content of surface species; structural parameters; comparisons of mass activity; percentages of Cu⁰, Cu⁺, and Cu²⁺ estimated by LCF; fitting parameters; textural parameters; and surface nitrogen compositions ([PDF](#))

AUTHOR INFORMATION

Corresponding Authors

Xiaofeng Yang – Collaborative Innovation Center of Chemistry for Energy Materials (iChEM), Dalian Institute of Chemical Physics and CAS Key Laboratory of Science and Technology on Applied Catalysis, Dalian Institute of Chemical Physics, Chinese Academy of Sciences, Dalian 116023, China;  orcid.org/0000-0001-5012-5651; Email: yangxf2003@dicp.ac.cn

Jian-Feng Li – Collaborative Innovation Center of Chemistry for Energy Materials (iChEM), College of Chemistry and Chemical Engineering, Xiamen University, Xiamen 361005, China;  orcid.org/0000-0003-1598-6856; Email: Li@xmu.edu.cn

Wei Liu – Division of Energy Research Resources, Dalian National Laboratory for Clean Energy, Dalian Institute of Chemical Physics, Chinese Academy of Sciences, Dalian 116023, China;  orcid.org/0000-0002-4403-737X; Email: weiliu@dicp.ac.cn

Aiqin Wang – Collaborative Innovation Center of Chemistry for Energy Materials (iChEM), Dalian Institute of Chemical Physics and CAS Key Laboratory of Science and Technology on Applied Catalysis, Dalian Institute of Chemical Physics, Chinese Academy of Sciences, Dalian 116023, China;  orcid.org/0000-0003-4552-0360; Email: aqwang@dicp.ac.cn

Authors

Ji Yang – Collaborative Innovation Center of Chemistry for Energy Materials (iChEM), Dalian Institute of Chemical Physics and CAS Key Laboratory of Science and Technology on Applied Catalysis, Dalian Institute of Chemical Physics, Chinese Academy of Sciences, Dalian 116023, China; Collaborative Innovation Center of Chemistry for Energy

Materials (iChEM), College of Chemistry and Chemical Engineering, Xiamen University, Xiamen 361005, China

Haiyong Qi – Collaborative Innovation Center of Chemistry for Energy Materials (iChEM), Dalian Institute of Chemical Physics and CAS Key Laboratory of Science and Technology on Applied Catalysis, Dalian Institute of Chemical Physics, Chinese Academy of Sciences, Dalian 116023, China

Anqi Li – Collaborative Innovation Center of Chemistry for Energy Materials (iChEM), Dalian Institute of Chemical Physics and CAS Key Laboratory of Science and Technology on Applied Catalysis, Dalian Institute of Chemical Physics, Chinese Academy of Sciences, Dalian 116023, China

Xiaoyan Liu – Collaborative Innovation Center of Chemistry for Energy Materials (iChEM), Dalian Institute of Chemical Physics and CAS Key Laboratory of Science and Technology on Applied Catalysis, Dalian Institute of Chemical Physics, Chinese Academy of Sciences, Dalian 116023, China;  orcid.org/0000-0003-2694-2306

Shengxin Zhang – Collaborative Innovation Center of Chemistry for Energy Materials (iChEM), Dalian Institute of Chemical Physics and CAS Key Laboratory of Science and Technology on Applied Catalysis, Dalian Institute of Chemical Physics, Chinese Academy of Sciences, Dalian 116023, China

Qiao Zhao – Division of Energy Research Resources, Dalian National Laboratory for Clean Energy, Dalian Institute of Chemical Physics, Chinese Academy of Sciences, Dalian 116023, China

Qike Jiang – Division of Energy Research Resources, Dalian National Laboratory for Clean Energy, Dalian Institute of Chemical Physics, Chinese Academy of Sciences, Dalian 116023, China

Yang Su – Collaborative Innovation Center of Chemistry for Energy Materials (iChEM), Dalian Institute of Chemical Physics and CAS Key Laboratory of Science and Technology on Applied Catalysis, Dalian Institute of Chemical Physics, Chinese Academy of Sciences, Dalian 116023, China

Leilei Zhang – Collaborative Innovation Center of Chemistry for Energy Materials (iChEM), Dalian Institute of Chemical Physics and CAS Key Laboratory of Science and Technology on Applied Catalysis, Dalian Institute of Chemical Physics, Chinese Academy of Sciences, Dalian 116023, China

Zhong-Qun Tian – Collaborative Innovation Center of Chemistry for Energy Materials (iChEM), College of Chemistry and Chemical Engineering, Xiamen University, Xiamen 361005, China;  orcid.org/0000-0002-9775-8189

Tao Zhang – Collaborative Innovation Center of Chemistry for Energy Materials (iChEM), Dalian Institute of Chemical Physics and CAS Key Laboratory of Science and Technology on Applied Catalysis, Dalian Institute of Chemical Physics, Chinese Academy of Sciences, Dalian 116023, China;  orcid.org/0000-0001-9470-7215

Complete contact information is available at:
<https://pubs.acs.org/10.1021/jacs.2c02262>

Author Contributions

¹J.Y., H.Q., and A.L. contributed equally to this work.

Notes

The authors declare no competing financial interest.

ACKNOWLEDGMENTS

Financial supports by the National Natural Science Foundation of China (22132006, 21776269, 21776271), LiaoNing Revitalization Talents Program (XLYC2007070), DNL Cooperation Fund, CAS (DNL202002), CAS Project for Young Scientists in Basic Research (YSBR-022), and the Youth Innovation Promotion Association CAS (2018216, 2022185, Y201828) are greatly acknowledged. We also thank the Beamline BL11B of the Shanghai Synchrotron Radiation Facility (SSRF) for providing sufficient beamline time.

REFERENCES

- (1) Gewirth, A. A.; Varnell, J. A.; DiAscro, A. M. Nonprecious Metal Catalysts for Oxygen Reduction in Heterogeneous Aqueous Systems. *Chem. Rev.* **2018**, *118*, 2313–2339.
- (2) Varela, A. S.; Ju, W.; Bagger, A.; Franco, P.; Rossmeisl, J.; Strasser, P. Electrochemical Reduction of CO₂ on Metal-Nitrogen-Doped Carbon Catalysts. *ACS Catal.* **2019**, *9*, 7270–7284.
- (3) Timoshenko, J.; Cuenya, B. R. *In Situ/Operando* Electrocatalyst Characterization by X-ray Absorption Spectroscopy. *Chem. Rev.* **2021**, *121*, 882–961.
- (4) Cao, L.; Luo, Q.; Liu, W.; Lin, Y.; Liu, X.; Cao, Y.; Zhang, W.; Wu, Y.; Yang, J.; Yao, T.; Wei, S. Identification of Single-Atom Active Sites in Carbon-Based Cobalt Catalysts during Electrocatalytic Hydrogen Evolution. *Nat. Catal.* **2019**, *2*, 134–141.
- (5) Li, J. K.; Sougrati, M. T.; Zitolo, A.; Ablett, J. M.; Oguz, I. C.; Mineva, T.; Matanovic, I.; Atanassov, P.; Huang, Y.; Zenyuk, I.; Di Cicco, A.; Kumar, K.; Dubau, L.; Maillard, F.; Drazic, G.; Jaouen, F. Identification of Durable and Non-Durable FeN_x Sites in Fe-N-C Materials for Proton Exchange Membrane Fuel Cells. *Nat. Catal.* **2021**, *4*, 10–19.
- (6) Lin, S.-C.; Chang, C.-C.; Chiu, S.-Y.; Pai, H.-T.; Liao, T.-Y.; Hsu, C.-S.; Chiang, W.-H.; Tsai, M.-K.; Chen, H. M. *Operando* Time-Resolved X-Ray Absorption Spectroscopy Reveals the Chemical Nature Enabling Highly Selective CO₂ Reduction. *Nat. Commun.* **2020**, *11*, 3525.
- (7) Jung, H.; Lee, S. Y.; Lee, C. W.; Cho, M. K.; Won, D. H.; Kim, C.; Oh, H.-S.; Min, B. K.; Hwang, Y. J. Electrochemical Fragmentation of Cu₂O Nanoparticles Enhancing Selective C-C Coupling from CO₂ Reduction Reaction. *J. Am. Chem. Soc.* **2019**, *141*, 4624–4633.
- (8) Huang, J.; Hörmann, N.; Oveisi, E.; Lojudice, A.; De Gregorio, G. L.; Andreussi, O.; Marzari, N.; Buonsanti, R. Potential-Induced Nanoclustering of Metallic Catalysts during Electrochemical CO₂ Reduction. *Nat. Commun.* **2018**, *9*, 3117.
- (9) Karapinar, D.; Huan, N. T.; Sahraie, N. R.; Li, J.; Wakerley, D.; Touati, N.; Zanna, S.; Taverna, D.; Tizei, L. H. G.; Zitolo, A.; Jaouen, F.; Mougel, V.; Fontecave, M. Electroreduction of CO₂ on Single-Site Copper-Nitrogen-Doped Carbon Material: Selective Formation of Ethanol and Reversible Restructuration of the Metal Sites. *Angew. Chem., Int. Ed.* **2019**, *58*, 15098–15103.
- (10) Weng, Z.; Wu, Y.; Wang, M.; Jiang, J.; Yang, K.; Huo, S.; Wang, X.-F.; Ma, Q.; Brudvig, G. W.; Batista, V. S.; Liang, Y.; Feng, Z.; Wang, H. Active Sites of Copper-Momplex Catalytic Materials for Electrochemical Carbon Dioxide Reduction. *Nat. Commun.* **2018**, *9*, 415.
- (11) Yang, J.; Liu, W.; Xu, M.; Liu, X.; Qi, H.; Zhang, L.; Yang, X.; Niu, S.; Zhou, D.; Liu, Y.; Su, Y.; Li, J.-F.; Tian, Z.-Q.; Zhou, W.; Wang, A.; Zhang, T. Dynamic Behavior of Single-Atom Catalysts in Electrocatalysis: Identification of Cu-N₃ as an Active Site for the Oxygen Reduction Reaction. *J. Am. Chem. Soc.* **2021**, *143*, 14530–14539.
- (12) Emsley, J. Going One Better than Nature? *Nature* **2001**, *410*, 633–634.
- (13) Foster, S. L.; Bakovic, S. I. P.; Duda, R. D.; Maheshwari, S.; Milton, R. D.; Minteer, S. D.; Janik, M. J.; Renner, J. N.; Greenlee, L. F. Catalysts for Nitrogen Reduction to Ammonia. *Nat. Catal.* **2018**, *1*, 490–500.
- (14) Gruber, N.; Galloway, J. N. An Earth-System Perspective of the Global Nitrogen Cycle. *Nature* **2008**, *451*, 293–296.
- (15) Wang, L.; Xia, M.; Wang, H.; Huang, K.; Qian, C.; Maravelias, C. T.; Ozin, G. A. Greening Ammonia toward the Solar Ammonia Refinery. *Joule* **2018**, *2*, 1055–1074.
- (16) Suryanto, B. H. R.; Du, H.-L.; Wang, D.; Chen, J.; Simonov, A. N.; MacFarlane, D. R. Challenges and Prospects in the Catalysis of Electroreduction of Nitrogen to Ammonia. *Nat. Catal.* **2019**, *2*, 290–296.
- (17) Wu, A.; Yang, J.; Xu, B.; Wu, X.-Y.; Wang, Y.; Lv, X.; Ma, Y.; Xu, A.; Zheng, J.; Tan, Q.; Peng, Y.; Qi, Z.; Qi, H.; Li, J.; Wang, Y.; Harding, J.; Tu, X.; Wang, A.; Yan, J.; Li, X. Direct Ammonia Synthesis from the Air via Gliding Arc Plasma Integrated with Single Atom Electrocatalysis. *Appl. Catal., B* **2021**, *299*, 120667.
- (18) Chen, H.; Yuan, D.; Wu, A.; Lin, X.; Li, X. Review of Low-Temperature Plasma Nitrogen Fixation Technology. *Waste Dispos. Sustain. Energy* **2021**, *3*, 201–217.
- (19) Butcher, D. P.; Gewirth, A. A. Nitrate Reduction Pathways on Cu Single Crystal Surfaces: Effect of Oxide and Cl⁻. *Nano Energy* **2016**, *29*, 457–465.
- (20) Wang, X.; Zhu, M.; Zeng, G.; Liu, X.; Fang, C.; Li, C. A Three-Dimensional Cu Nanobelt Cathode for Highly Efficient Electrocatalytic Nitrate Reduction. *Nanoscale* **2020**, *12*, 9385–9391.
- (21) Zeng, Y.; Priest, C.; Wang, G.; Wu, G. Restoring the Nitrogen Cycle by Electrochemical Reduction of Nitrate: Progress and Prospects. *Small Methods* **2020**, *4*, 2000672.
- (22) Zhu, T.; Chen, Q.; Liao, P.; Duan, W.; Liang, S.; Yan, Z.; Feng, C. Single-Atom Cu Catalysts for Enhanced Electrocatalytic Nitrate Reduction with Significant Alleviation of Nitrite Production. *Small* **2020**, *16*, 2004526.
- (23) Chen, G.-F.; Yuan, Y.; Jiang, H.; Ren, S.-Y.; Ding, L.-X.; Ma, L.; Wu, T.; Lu, J.; Wang, H. Electrochemical Reduction of Nitrate to Ammonia via Direct Eight-Electron Transfer using a Copper-Molecular Solid Catalyst. *Nat. Energy* **2020**, *5*, 605–613.
- (24) Wu, Z.-Y.; Karamad, M.; Yong, X.; Huang, Q.; Cullen, D. A.; Zhu, P.; Xia, C.; Xiao, Q.; Shakouri, M.; Chen, F.-Y.; Kim, J. Y.; Xia, Y.; Heck, K.; Hu, Y.; Wong, M. S.; Li, Q.; Gates, I.; Siahrostami, S.; Wang, H. Electrochemical Ammonia Synthesis via Nitrate Reduction on Fe Single Atom Catalyst. *Nat. Commun.* **2021**, *12*, 2870.
- (25) Rajmohan, K. S.; Chetty, R. Enhanced Nitrate Reduction with Copper Phthalocyanine-Coated Carbon Nanotubes in a Solid Polymer Electrolyte Reactor. *J. Appl. Electrochem.* **2016**, *47*, 63–74.
- (26) Li, P.; Jin, Z.; Fang, Z.; Yu, G. A Single-Site Iron Catalyst with Preoccupied Active Centers That Achieves Selective Ammonia Electrosynthesis from Nitrate. *Energy Environ. Sci.* **2021**, *14*, 3522–3531.
- (27) Rehr, J. J.; Albers, R. C. Theoretical Approaches to X-Ray Absorption Fine Structure. *Rev. Mod. Phys.* **2000**, *72*, 621–654.
- (28) Joly, Y. X-ray Absorption Near-Edge Structure Calculations beyond the Muffin-Tin Approximation. *Phys. Rev. B: Condens. Matter Mater. Phys.* **2001**, *63*, 125120.
- (29) Bunău, O.; Joly, Y. Self-Consistent Aspects of X-Ray Absorption Calculations. *J. Phys.: Condens. Matter* **2009**, *21*, 345501.
- (30) Wang, Y.; Zhou, W.; Jia, R.; Yu, Y.; Zhang, B. Unveiling the Activity Origin of a Copper-based Electrocatalyst for Selective Nitrate Reduction to Ammonia. *Angew. Chem., Int. Ed.* **2020**, *59*, 5350–5354.
- (31) Fu, X.; Zhao, X.; Hu, X.; He, K.; Yu, Y.; Li, T.; Tu, Q.; Qian, X.; Yue, Q.; Wasielewski, M. R.; Kang, Y. Alternative Route for Electrochemical Ammonia Synthesis by Reduction of Nitrate on Copper Nanosheets. *Appl. Mater. Today* **2020**, *19*, 100620.
- (32) Gong, Z.; Zhong, W.; He, Z.; Liu, Q.; Chen, H.; Zhou, D.; Zhang, N.; Kang, X.; Chen, Y. Regulating Surface Oxygen Species on Copper(I) Oxides via Plasma Treatment for Effective Reduction of Nitrate to Ammonia. *Appl. Catal., B* **2022**, *305*, 121021.
- (33) Wang, H.; Mao, Q.; Ren, T.; Zhou, T.; Deng, K.; Wang, Z.; Li, X.; Xu, Y.; Wang, L. Synergism of Interfaces and Defects: Cu/Oxygen Vacancy-Rich Cu-Mn₃O₄ Heterostructured Ultrathin Nanosheet

- Arrays for Selective Nitrate Electroreduction to Ammonia. *ACS Appl. Mater. Interfaces* **2021**, *13*, 44733–44741.
- (34) Wu, H.; Li, H.; Zhao, X.; Liu, Q.; Wang, J.; Xiao, J.; Xie, S.; Si, R.; Yang, F.; Miao, S.; Guo, X.; Wang, G.; Bao, X. Highly Doped and Exposed Cu(I)-N Active Sites Within Graphene towards Efficient Oxygen Reduction for Zinc-Air Batteries. *Energy Environ. Sci.* **2016**, *9*, 3736–3745.
- (35) Giri, S. D.; Sarkar, A. Electrochemical Study of Bulk and Monolayer Copper in Alkaline Solution. *J. Electrochem. Soc.* **2016**, *163*, H252–H259.
- (36) Fang, S.; Zhu, X.; Liu, X.; Gu, J.; Liu, W.; Wang, D.; Zhang, W.; Lin, Y.; Lu, J.; Wei, S.; Li, Y.; Yao, T. Uncovering Near-Free Platinum Single-Atom Dynamics during Electrochemical Hydrogen Evolution Reaction. *Nat. Commun.* **2020**, *11*, 1029.
- (37) Su, H.; Zhou, W.; Zhang, H.; Zhou, W.; Zhao, X.; Li, Y.; Liu, M.; Cheng, W.; Liu, Q. Dynamic Evolution of Solid-Liquid Electrochemical Interfaces over Single-Atom Active Sites. *J. Am. Chem. Soc.* **2020**, *142*, 12306–12313.
- (38) Ma, L.; Hu, W.; Mei, B.; Liu, H.; Yuan, B.; Zang, J.; Chen, T.; Zou, L.; Zou, Z.; Yang, B.; Yu, Y.; Ma, J.; Jiang, Z.; Wen, K.; Yang, H. Covalent Triazine Framework Confined Copper Catalysts for Selective Electrochemical CO₂ Reduction: *Operando* Diagnosis of Active Sites. *ACS Catal.* **2020**, *10*, 4534–4542.
- (39) Yi, J. D.; Xie, R.; Xie, Z. L.; Chai, G. L.; Liu, T. F.; Chen, R. P.; Huang, Y. B.; Cao, R. Highly Selective CO₂ Electroreduction to CH₄ by In Situ Generated Cu₂O Single-Type Sites on a Conductive MOF: Stabilizing Key Intermediates with Hydrogen Bonding. *Angew. Chem., Int. Ed.* **2020**, *59*, 23641–23648.
- (40) Ko, W.-Y.; Chen, W.-H.; Cheng, C.-Y.; Lin, K.-J. Architectural Growth of Cu Nanoparticles Through Electrodeposition. *Nanoscale Res. Lett.* **2009**, *4*, 1481–1485.
- (41) Lum, Y.; Ager, J. W. Stability of Residual Oxides in Oxide-Derived Copper Catalysts for Electrochemical CO₂ Reduction Investigated with ¹⁸O Labeling. *Angew. Chem., Int. Ed.* **2017**, *57*, 551–554.
- (42) Johnston, S.; Kemp, L.; Turay, B.; Simonov, A. N.; Suryanto, B. H. R.; MacFarlane, D. R. Copper-Catalyzed Electrosynthesis of Nitrite and Nitrate from Ammonia: Tuning the Selectivity via an Interplay Between Homogeneous and Heterogeneous Catalysis. *ChemSusChem* **2021**, *14*, 4793–4801.
- (43) Zhao, X.; Jia, X. X.; He, Y. N.; Zhang, H. B.; Zhou, X. H.; Zhang, H. C.; Zhang, S. S.; Dong, Y. M.; Hu, X.; Kuklin, A. V.; Baryshnikov, G. V.; Ågren, H.; Hu, G. Z. Two-Dimensional BCN Matrix Inlaid with Single-Atom-Cu Driven Electrochemical Nitrate Reduction Reaction to Achieve Sustainable Industrial-Grade Production of Ammonia. *Appl. Mater. Today* **2021**, *25*, 101206.

□ Recommended by ACS

Roles of Copper in Nitrate Reduction at Copper-Modified Ru/C Catalysts

Jia-Qi Chen, Yan-Xia Chen, et al.

FEBRUARY 01, 2023

THE JOURNAL OF PHYSICAL CHEMISTRY C

READ ↗

Combined Effects of Concentration, pH, and Polycrystalline Copper Surfaces on Electrocatalytic Nitrate-to-Ammonia Activity and Selectivity

Luisa Barrera, Rohini Bala Chandran, et al.

MARCH 13, 2023

ACS CATALYSIS

READ ↗

Cu₂O–Cu@Titanium Surface with Synergistic Performance for Nitrate-to-Ammonia Electrochemical Reduction

Marcelo Eduardo Chavez, Joan Ramon Morante, et al.

FEBRUARY 22, 2023

ACS SUSTAINABLE CHEMISTRY & ENGINEERING

READ ↗

Insights into Electrocatalytic Nitrate Reduction to Ammonia via Cu-Based Bimetallic Catalysts

Jing Zhao, Lilong Jiang, et al.

FEBRUARY 01, 2023

ACS SUSTAINABLE CHEMISTRY & ENGINEERING

READ ↗

Get More Suggestions >